Simulation of Linear Switched Reluctance Motor Drives

Jordi Garcia Amorós [1] , Balduí Banqué Molina [2], Pere Andrada Gascón [2]

1 Departament d'Enginyeria Electrònica, Eléctrica i Automàtica
E.T.S.E., Universitat Rovira i Virgili
Avinguda Països Catalans, 26, 43007 Tarragona, Spain
Tel.:+34 977 559695, fax:+34 977559605
E-mail: jordi.garcia-amoros@urv.cat
URL: http://sauron.etse.urv.es/DEEEA/

[2] **GAECE.** Grup d'Accionamients Elèctrics amb Commutació Electrònica
Departament d'Enginyeria Elèctrica, EPSEVG-UPC
Víctor Balaguer 1, 08800 Vilanova i la Geltrú, Spain
Tel.:+34 938967732; fax: +34 938967700
E-mail: blanque@ee.upc.edu
E-mail: pere.andrada@ upc.edu

Abstract

This paper presents a simulation model of linear switched reluctance motor drives. A *Matlab-Simulink* environment coupled with finite element analysis is used to perform the simulations. Experimental and simulation results for a double sided linear switched motor drive prototype are reported and compared to verify the simulation model.

Keywords

«Electrical machine», «Switched reluctance drive», «Linear drive», «Modelling»

Introduction

Linear motors are direct electromagnetic drives in which the linear motion is generated without intermediary mechanical gearboxes or belts. Despite their lower force/weight ratio [1], linear switched reluctance motors (LSRMs) are an attractive alternative to other linear motors because they only have concentrated windings on the stator or translator, they are ruggedly built, have low expected manufacturing costs, and have fault tolerance capability. There are many applications that require LSRMs, and they can be found in propulsion systems for railway vehicles or vertical elevators [2,3] or in precise motion control for packaging machines or material handling equipment [4,5]. LSRMs are classified according to the relation between the position of the plane that contains the flux lines and the direction of the movement; that is, they are longitudinal flux LSRMs if they are parallel and transverse flux LSRMs if they are perpendicular. Longitudinal LSRMs may be tubular or flat. There are different types of longitudinal flat LSRMs: the simplest is the single-sided flat LSRM shown in Fig.1, whereas others are more complex, such as the double-sided flat LSRM and the modified doubled-sided SRM that are depicted in Fig.2

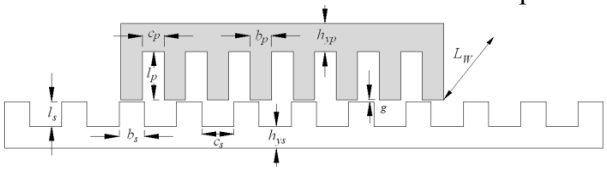

Fig. 1. Main dimensions of a single-sided longitudinal flat LSRM

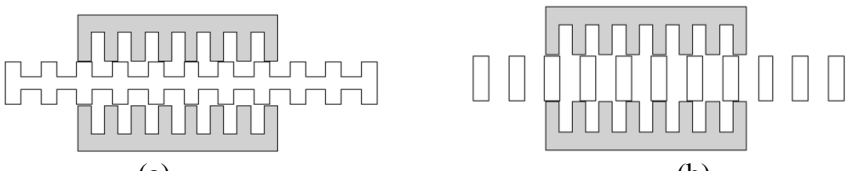

(a) (b)

Fig. 2. Other types of longitudinal flat LSRMs: a) Conventional double-sided, b) Modified double-sided

Many papers have dealt with modeling and simulation switched reluctance motor drives [6-8] but, until now, little work has been done in their linear counterpart. This paper is devoted to the simulation of the whole LSRM drive, including the linear motor, the power converter and the control. The proposed simulation model is intended as a useful and reliable tool for the computer-aided design of any reluctance linear motor. A *Matlab-Simulink* environment coupled with finite element analysis is used to perform the simulations. Experimental and simulation results for a double sided linear switched motor drive prototype are reported and compared in order to verify the simulation model.

Non-linear mathematical model of LSRM

The voltage equation of a stator phase of an *m*-phases LSRM is:

$$u = R\cdot i + \frac{\partial \psi(x,i)}{\partial t} = R\cdot i + \frac{\partial \psi(x,i)}{\partial i}\cdot\frac{d i}{d t} + \frac{\partial \psi(x,i)}{\partial x}\cdot v \tag{1}$$

Figure 3 shows the electrical equivalent circuit of a stator phase of an LSRM, in which u is the DC bus voltage, i is the phase current, R is the phase resistance, L_{INC} is the incremental inductance and e_m is the back electromotive force to the translator movement at velocity v.

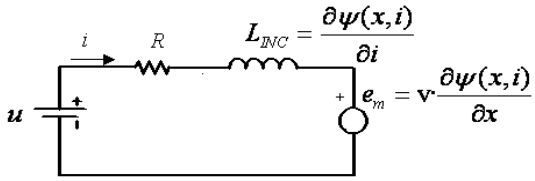

Fig. 3. Single phase equivalent electric circuit of an LSRM

Thus equation (1) can be rewritten in the form:

$$u = R\cdot i + L_{INC}\cdot\frac{d i}{d t} + e_m \tag{2}$$

The instantaneous electromagnetic force of one phase is computed in terms of the differential change of co-energy with respect to position, which is evaluated at a constant phase current. The total electromagnetic force, neglecting mutual inductance effects, is obtained by:

$$F_e = \sum_{i=1}^{m}\left(\frac{\partial}{\partial x}\left(\int_0^I \psi(x,i)\, d i\right)\Bigg|_{i=ctn}\right) \tag{3}$$

The coupling force equation between motor and load is given by:

$$F_e = m\cdot\frac{d v}{d t} + B\cdot v + F_L \tag{4}$$

Where m_t is the mass, B is the viscous friction coefficient and F_L is the external load force. Rearranging equations (2), (3) and (4), the state-space equations are described by (5) and (6).

$$\frac{d i}{d t} = \left(\frac{\partial \psi(x,i)}{\partial i}\right)^{-1}\cdot\left(u - R\cdot i - \frac{\partial \psi(x,i)}{\partial x}\cdot v\right) \tag{5}$$

$$\frac{d v}{d t} = \frac{1}{m}\cdot\left(F_e - F_L - B\cdot v\right) \tag{6}$$

Matlab/Simulink® simulation model

The simulation model of the LSRM drive consists of three modules: the LSRM module, the power converter module and the controller module (see Figure 4). The LSRM module models the electrical and mechanical equations of the LSRM. The power converter module models the power converter logic switching. The controller module generates the drive signals according to the reference signals, translator position and phase currents depending on external load force.

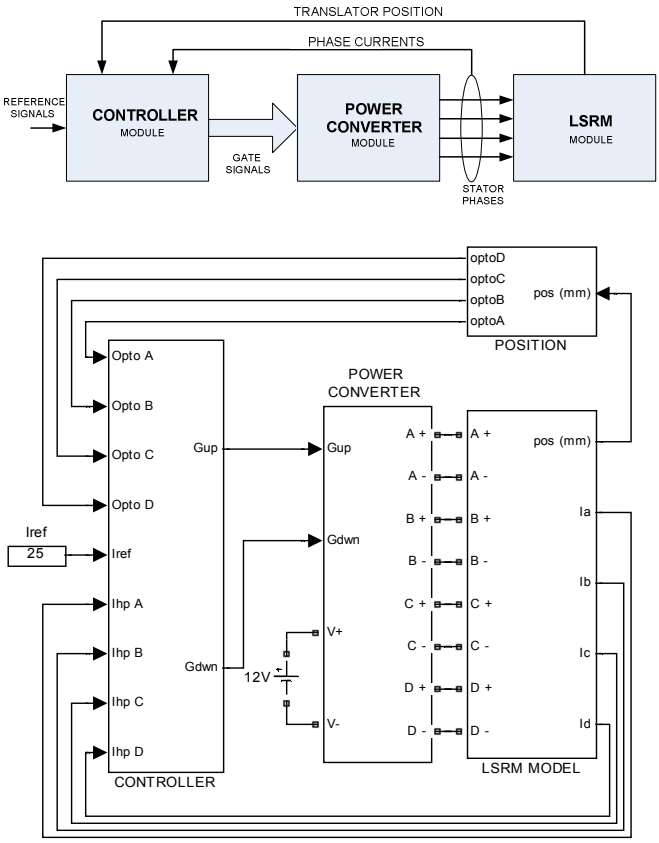

Fig. 4. Block diagram (above in grey). *Simulink* complete block model (below)

1. LSRM module

The LSRM module shown in Fig. 5 simulates the system of equations (5)-(6).

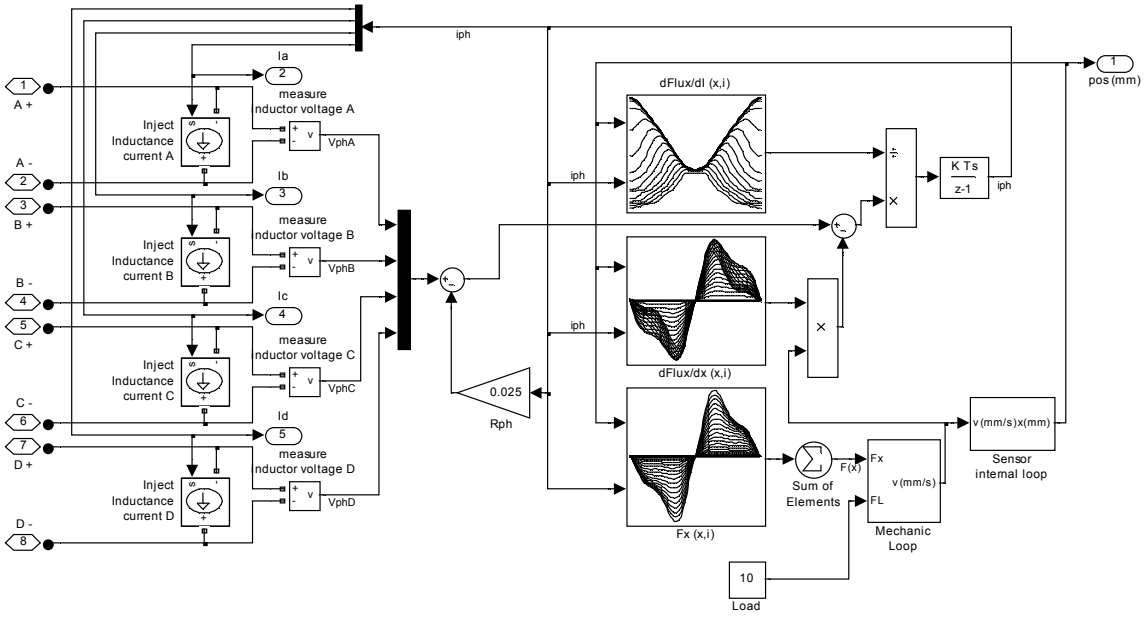

Fig. 5. LSRM module

The flux linked–current characteristics, or magnetization curves, $\psi = \psi(x,i)$ and the electromagnetic force $F_e = F(x,i)$ are obtained by two-dimensional finite element analysis in order to reduce the computing time, and corrected using the end-effects coefficient, K_{ee} to account for the end effects, depending on the current density (J) and position (x) given by [9] [10]:

$$\psi_{3D} = K_{ee} \cdot \psi_{2D} \tag{7}$$

$$L_{3D} = K_{ee} \cdot L_{2D} \tag{8}$$

Where Ψ_{2D} and L_{2D} are the flux linkage and the inductance obtained in 2D FEA and where Ψ_{3D} and L_{3D} are the 3D flux linkage and the inductance approaches that account for the end effects and are most similar to the measured values. The correction factor K_{ee} is defined as: [11]

$$K_{ee} = \left(1 + \frac{L_{end}}{L_{2D}}\right) \cdot K_f \tag{9}$$

Where L_{end} is the end-winding inductance and K_f is the axial fringing factor. End-winding inductance, $L_{end,}$ can be analytically deduced from end-winding geometry or can be computed by means of an axis-symmetrical 2D finite element model.

Given (Ψ_{3D}), the co-energy (W'_{3D}) is calculated using the well-known expression:

$$W'_{3D}(x_i, I) = \int_o^I \psi_{3D}(x, i) \cdot di \Big|_{x_i = Ctn} \tag{10}$$

Then, the translation force, including the end effects, is obtained by:

$$F_{X,3D}(x, I) = \frac{\partial W'_{3D}(x, I)}{\partial x}\Big|_{I=Ctn} \tag{11}$$

For small intervals of position (Δx) and current (ΔI) a practical expression of (11) can be given by:

$$F_{X,3D}(x, I) \approx \frac{\Delta W'}{\Delta x} = \frac{\Delta I}{\Delta x} \cdot \left[\sum_0^I \psi_{3D}(x + \Delta x, I) - \sum_0^I \psi_{3D}(x, I) \right] \tag{12}$$

Once the magnetization curves have been obtained using the aforementioned procedure, the partial derivatives $\partial \psi(x,i)/\partial i$ and $\partial \psi(x,i)/\partial x$ are determined numerically.

2. Power converter module

This module models the power converter, in this case a four phase asymmetric half-bridge or classical converter (Fig. 6). The converter is modeled using the available power semiconductor devices from the *SimPowerSystems* toolbox (IGBT and diode). Some of the critical settings for IGBTs, such as the falling time (t_f) and the tail time (t_t), are taken into account because a failure to properly select these parameters would produce a high peak voltage, especially for high switching frequencies. The module also includes the model of the *snubber* which is required for the power converter to behave correctly.

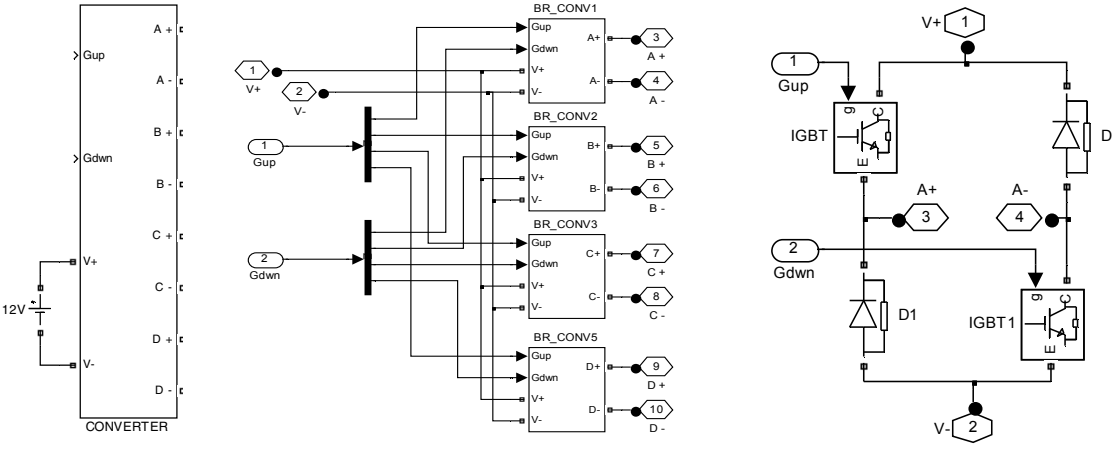

Fig. 6. Power converter module (left). Power converter detail (center). Phase detail (right)

3. Controller module

Depending on the external load force, this module generates the drive signals according to the reference signals, translator position and phase currents (Fig. 7). This module performs two main functions. The first is to implement the adopted control strategy which can range from a simple sequential control of the different phases to a sophisticated control that uses force distribution functions to reduce propulsion force pulsations. The second is to generate the drive signals according to the control strategy and to decide which current regulator is to be employed (single pulse, or soft chopping and hard chopping hysteresis).

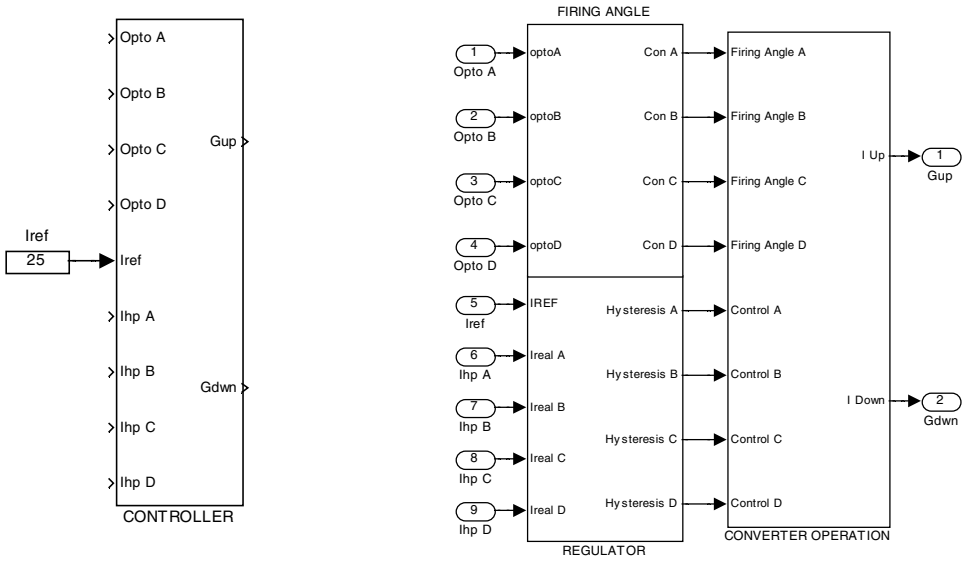

Fig. 7. Controller module (left), controller module detail (right)

Simulation and experimental results

In order to verify the proposed procedure a four phase double-sided LSRM drive prototype has been designed, built and tested (Fig. 8). The power converter is a four phase classic converter (Fig 9). The control is a sequential phase control designed to apply a precision linear motion using a soft chopping current regulator.

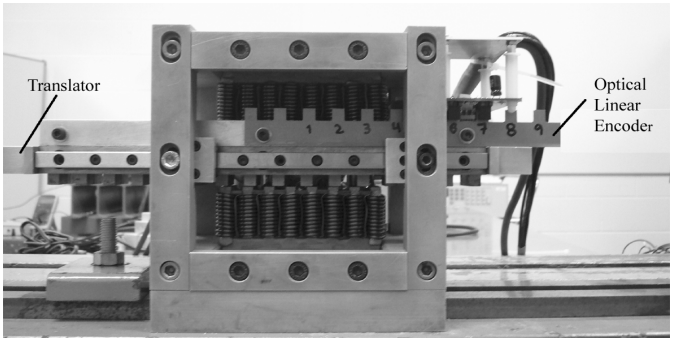

Fig. 8. LSRM prototype

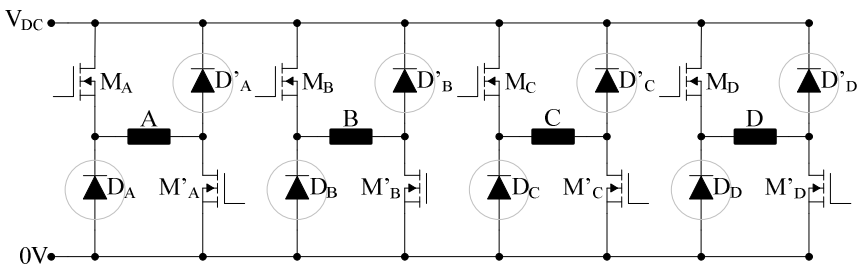

Fig. 9. Block diagram of the four phase classic converter

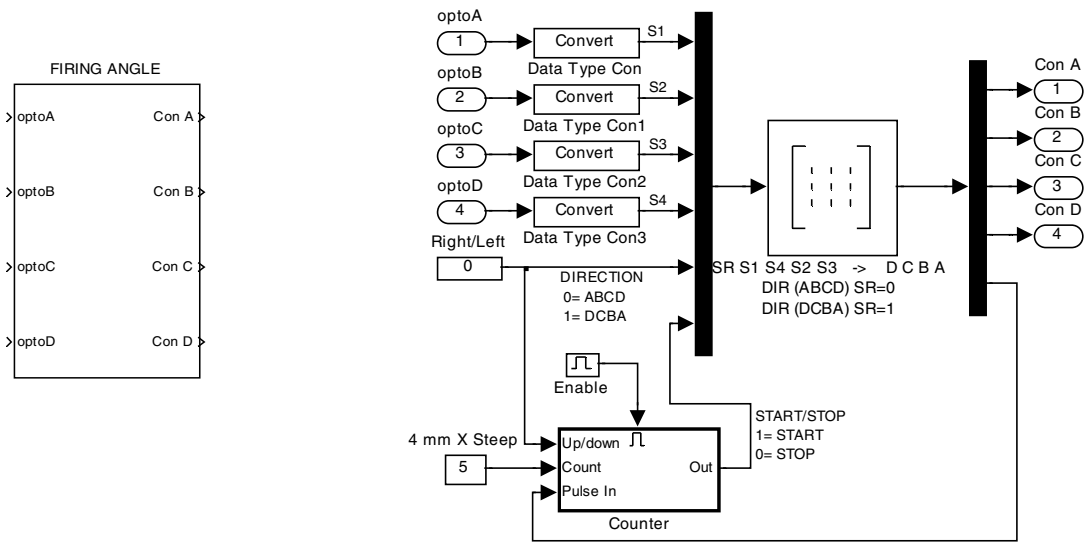

Fig. 10. Firing angle module for the application case

In this case, the firing angle generator (Fig.10) is implemented by a truth table and a counter. In the truth table, the switching sequences of the motor phases have been programmed taking into account the position of the translator, which is obtained by means of four optoelectronic switches. It is possible to choose the direction of the movement and the number of steps (variable Step 5, which includes 5 steps with a resolution of 4mm). The truth table also generates 4mm pulses which are obtained by combining the optoelectronic switch signals. The counter counts these pulses when "Enable" is activated, thus generating "1" in the output, and "0" as soon as the count has finished because the outputs remain at "0" when "START / STOP" is set to "0".

1. Finite element simulation.

The prototype has been analysed using the finite element method (FEM) and taking into account the end effects. Flux and density plots for the aligned and unaligned positions are shown in Figs.11 and 12 respectively. The analysis has been carried out between two unaligned positions x=-S and x=S, where S is the distance between the aligned and unaligned positions given by $S = (c_s+b_s)/2$ (see Fig. 1).

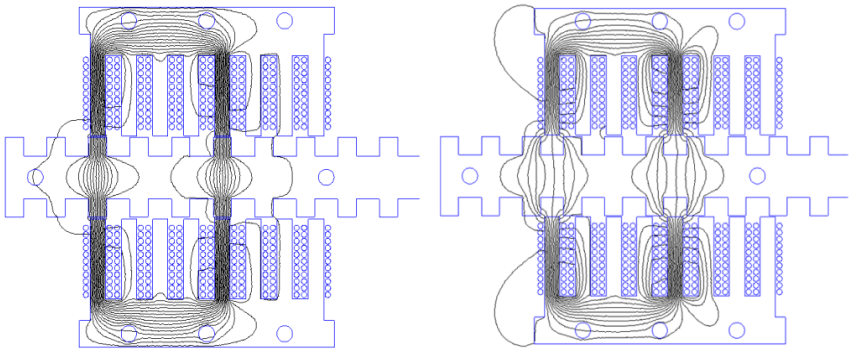

(a) (b)

Fig. 11. Flux plots from 2D FEA of the LSRM a) aligned $x = S$. b) unaligned $x = 0$.

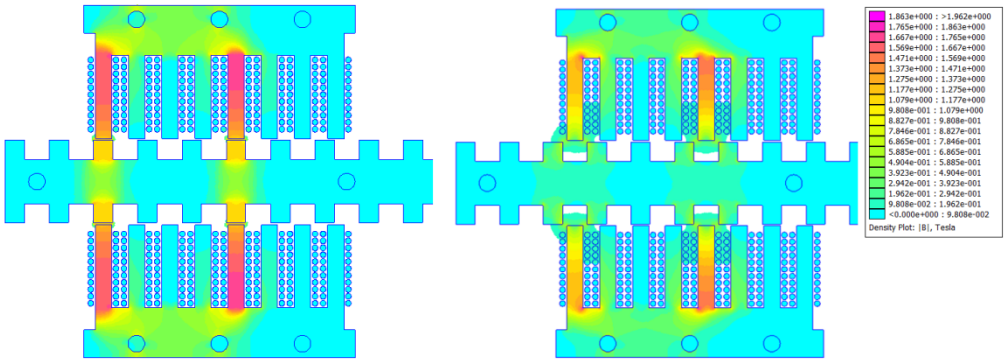

(a) (b)

Fig. 12. Flux density plots from 2D FEA of the LSRM a) aligned $x = S$. b) unaligned $x = 0$.

The magnetization curve (ψ_{3D}) shown in Fig. 13a has been obtained from 2D-FEM analysis and corrected by (7) to account for end-effects. The force is obtained by taking ψ_{3D} and applying (12) (Fig. 13b). The partial derivatives $\partial\psi(x,i)/\partial i$ and $\partial\psi(x,i)/\partial x$ are shown in Fig 12c and 12d respectively

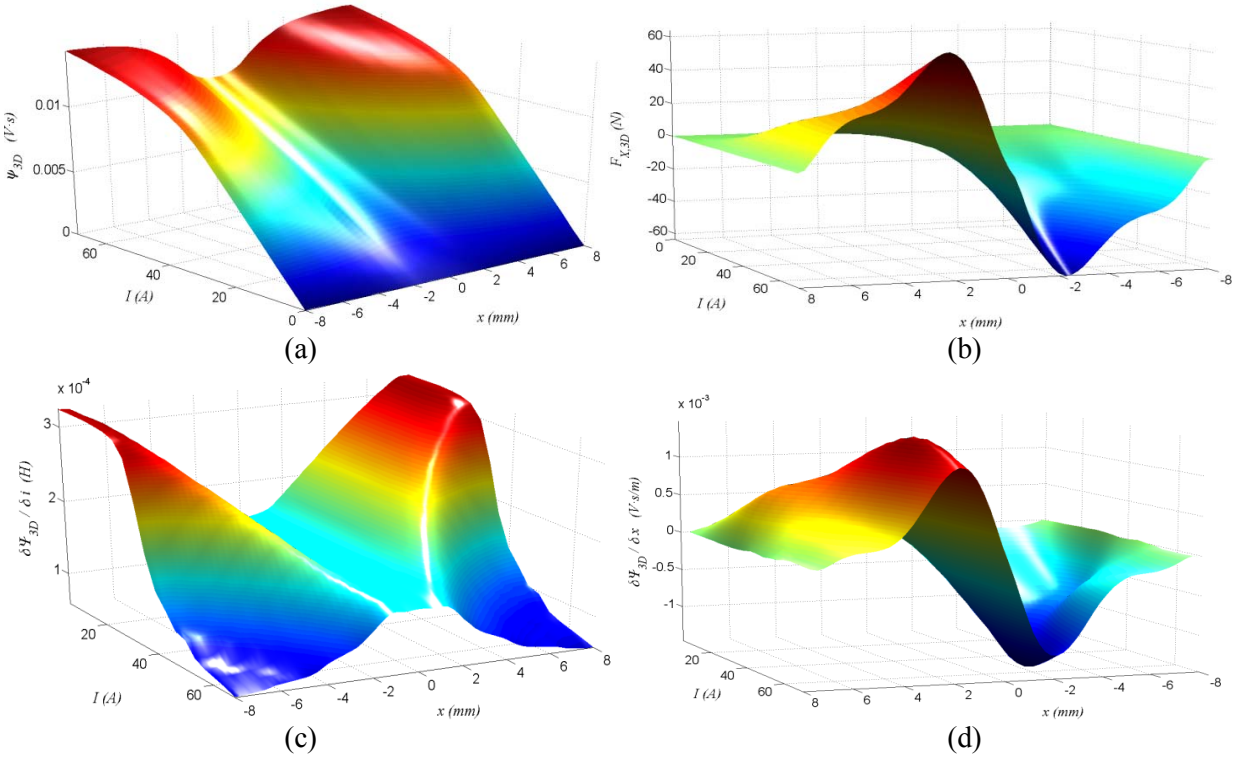

Fig. 13. FEM results plots for position $x \in [-S,S]=[-8,8]$ and current $I \in [0,69]$.

2. Simulation and measurement: comparison results

The simulation results of the proposed model are compared with waveforms measured from experiments. Fig 14 shows the measured and simulated position and phase currents. Fig 15 shows the measured and simulated phase current and phase voltage.

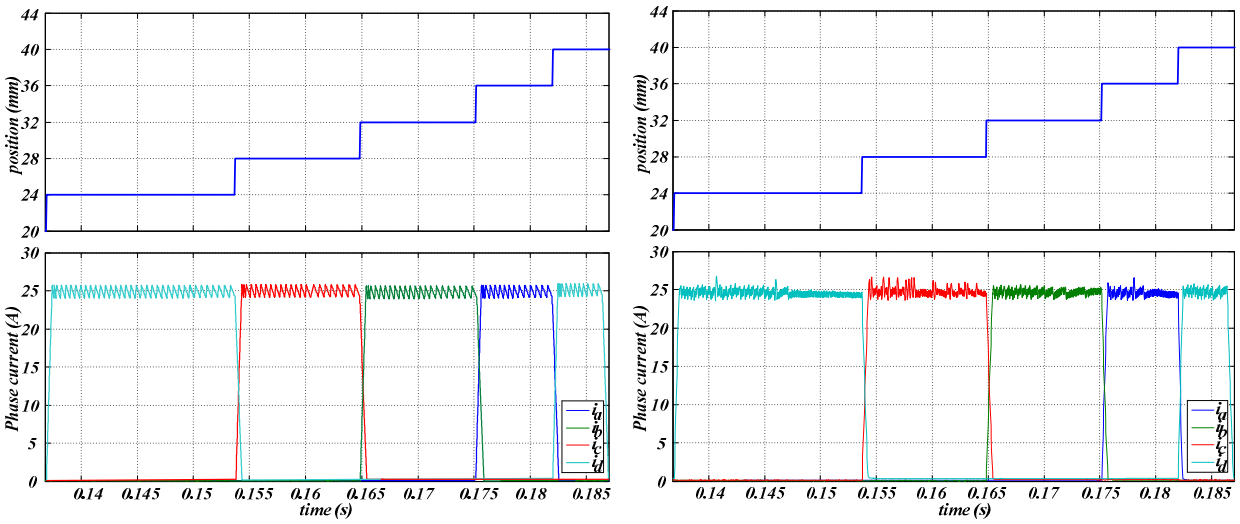

Fig. 14. Position and phase current obtained by simulation (left) and by measurement (right)

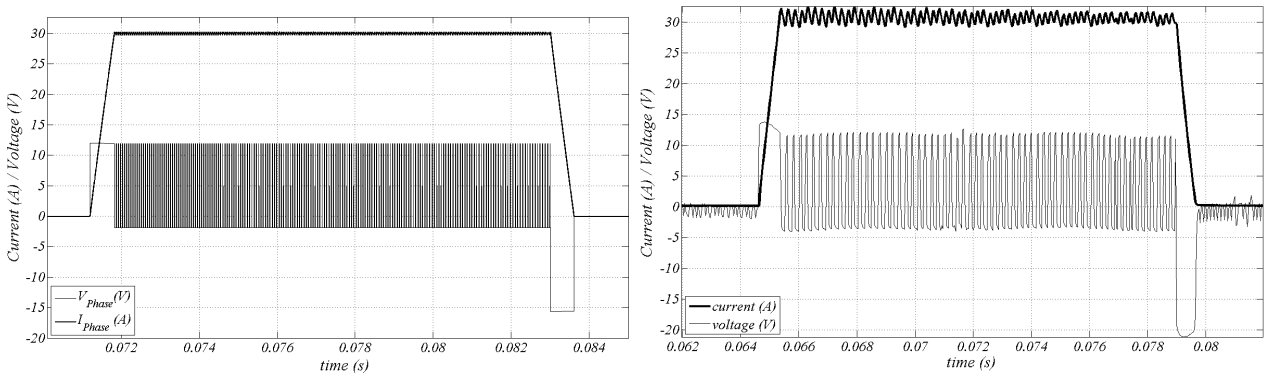

Fig. 15. Phase current and phase voltage obtained by simulation (left) and by measurement (right)

Conclusions

This paper presents a new LSRM simulation model. This model has three independent modules: the controller module, the power converter module and the LSRM module. This enables it to be used in other types of reluctance motors and for different control strategies. The paper also presents a particular application for an LSRM. The experimental results obtained agree with the simulation results, which in turn validate the LSRM model.

References

[1] Bianchi, N.; Bolognani, S.; Corda, J.; "Tubular linear motors: a comparison of brushless PM and SR motors", International Conference on Power Electronics, Machines and Drives, 2002. (Conf. Publ. No. 487), vol., no., pp. 626-631, 4-7 June 2002

[2] Kolomeitsev L., Kraynov D., Pakhomin F., Kallenbach E., Kireev V., Schneider T., Böcker J. "Linear Switched Reluctance Motor as High Efficiency Propulsion System for Railway Vehicles" SPEEDAM 2008 pp 155-160.

[3] Lobo N.S., Honh Sun Lim, Krishnan R. "Comparison of Linear Switched Reluctance Machines for Vertical Propulsion Application: Analysis, Design, and Experimental Correlation". IEEE Transactions on Industry Applications, Vol. 44, No 4 July/August 2008, pp 1134-1142

[4] Pan J., Cheung N.C., Jinming Yang, "High-precision position control of a novel planar switched reluctance motor", IEEE Transactions on Industrial Electronics, vol.52, no.6, pp. 1644-1652, Dec. 2005

[5] Zhao S. W., Cheung, N.C., Wai-Chuen Gan; Jin Ming Yang; Jian Fei Pan, "A Self-Tuning Regulator for the High-Precision Position Control of a Linear Switched Reluctance Motor", IEEE Transactions on Industrial Electronics , vol.54, no.5, pp.2425-2434, Oct. 2007

[6] F. D'hulster, R.Stockman, R.J.M. Belmans. "Modelling of Switched Reluctance Machines: State of Art". International Journal of Modelling and Simulation. Vol 4, 2004, pp 214-223.

[7] I.Husain, S.A.Hossain. "Modelling, Simulation, and Control of Switched Reluctance Motor Drives". IEEE Transactions on Industry Electronics, Vol, 53, No 6, pp 1625-1634, December 2005.

[8] K.F. Wong, K.W.E. Cheng, S.L.Ho. "Simulation of Switched Reluctance Motor Based on a Combination of Circuit-oriented and Signal-oriented Approaches Using Matlab/SimPowerSystems". Electric Power Components and ystems,35, 2005-219, 2007.

[9] D'hulster F., Stockman K., Belmans R. J. M., "Modelling of Switched Reluctance Machines: State of the Art" International Journal of Modelling and Simulation, vol. 24, no. 4, pp. 216-223, 2004

[10] Matveev A., Kuzmichev V., Lomonova E., "A new comprehensive approach to estimation of end-effects in switched reluctance motors", Proceedings ICEM2002, Bruges, Belgium, August 2002

[11] Amoros, J. G.; Andrada, P., "Sensitivity Analysis of Geometrical Parameters on a Double-Sided Linear Switched Reluctance Motor", IEEE Transactions on Industrial Electronics, vol.57, no.1, pp.311-319, January. 2010

Annex

Table I. LSRM prototype main parameters

Primary pole width	b_p	*6 mm*
Primary slot width	c_p	*6 mm*
Primary pole pitch	T_p	*12 mm*
Number of active poles per side	N_p	*8*
Primary pole length	l_p	*30 mm*
Secondary pole width	b_s	*7 mm*
Secondary slot width	c_s	*9 mm*
Secondary pole pitch	T_s	*16 mm*
Number of passive poles per side	N_s	*6*
Secondary pole length	l_s	*7 mm*
Yoke length	h_y	*8 mm*
Stack length	L_W	*30 mm*
Number of turns per pole	N_l	*11*
Wire diameter	d_c	*2.1 mm*

The viscous friction coefficient, *B,* can be evaluated by $B=v\cdot\rho\cdot A/y$, where v is the kinematic viscosity ($m^2\cdot s^{-1}$), ρ is the hydraulic fluid density ($kg\cdot m^{-3}$), A is the contact surface (m^2) and y is the clearance occupied by the hydraulic fluid (m). Usually, for hydraulic fluids, $v = 64\cdot10^{-6}\ m^2\cdot s^{-1}$ and $\rho = 800\ kg\cdot m^{-3}$. When linear bearings are used, friction force becomes $F_r=g\cdot m_s\cdot\mu$, where g is the standard gravity constant ($9.80665 m\cdot s^{-2}$), m_s is the mass supported by the bearings (kg) and μ is the non dimensional rolling friction coefficient. For linear bearings with recirculating balls $\mu = 0.005$.